Conductive hydrogel based on chitosan-aniline pentamer/gelatin/agarose significantly promoted motor neuron-like cells differentiation of human olfactory ecto-mesenchymal stem cells

Materials Science & Engineering C 101 (2019) 243–253

Contents lists available at ScienceDirect

Materials Science & Engineering C

journal homepage: www.elsevier.com/locate/msec

Conductive hydrogel based on chitosan-aniline pentamer/gelatin/agarose significantly promoted motor neuron-like cells differentiation of human olfactory ecto-mesenchymal stem cells

Zohreh Bagher[a], Zhaleh Atoufi[b], Rafieh Alizadeh[a], Mohammad Farhadi[a], Payam Zarrintaj[c], Lorenzo Moroni[d], Mohsen Setayeshmehr[d,e], Ali Komeili[f], S. Kamran Kamrava[f,a,*]

[a] ENT and Head & Neck Research Center and Department, The Five Senses Institute, Hazrat Rasoul Akram Hospital, Iran University of Medical Sciences, Tehran, Iran
[b] School of Chemical Engineering, College of Engineering, University of Tehran, Tehran, Iran
[c] Polymer Engineering Department, Faculty of Engineering, Urmia University, Urmia, Iran
[d] MERLN Institute for Technology Inspired Regenerative Medicine, Complex Tissue Regeneration, Maastricht University, Maastricht, the Netherlands
[e] Department of Tissue Engineering and Regenerative Medicine, Faculty of Advance Technologies in Medicine, Iran University of Medical Sciences, Tehran, Iran
[f] Applied Biophotonics Research Center, Science and Research Branch, Islamic Azad University, Tehran, Iran

ARTICLE INFO

Keywords:
Conductive polymers
Aniline pentamer
Motor neuron differentiation
Nasal ectomesenchymal stem cells

ABSTRACT

Developing a simple produces for efficient derivation of motor neurons (MNs) is essential for neural tissue engineering studies. Stem cells with high capacity for neural differentiation and scaffolds with the potential to promote motor neurons differentiation are promising candidates for neural tissue engineering. Recently, human olfactory ecto-mesenchymal stem cells (OE-MSCs), which are isolated easily from the olfactory mucosa, are considered a new hope for neuronal replacement due to their neural crest origin. Herein, we synthesized conducting hydrogels using different concentration of chitosan-g-aniline pentamer, gelatin, and agarose. The chemical structures, swelling and deswelling ratio, ionic conductivity and thermal properties of the hydrogel were characterized. Scaffolds with 10% chitosan-g-aniline pentamer/gelatin (S10) were chosen for further investigation and the potential of OE-MSCs as a new source for programming to motor neuron-like cells investigated on tissue culture plate (TCP) and conductive hydrogels. Cell differentiation was evaluated at the level of mRNA and protein synthesis and indicated that conductive hydrogels significantly increased the markers related to motor neurons including Hb-9, Islet-1 and ChAT compared to TCP. Taken together, the results suggest that OE-MSCs would be successfully differentiated into motor neuron-like cells on conductive hydrogels and would have a promising potential for treating motor neuron-related diseases.

1. Introduction

Motor neurons (MNs) are known as a typical class of neurons that are located in the central nervous system and project their axons to control muscular activity [1]. They are damaged in motor neuron-related diseases such as amyotrophic lateral sclerosis and spinal cord injuries [2]. Replacement of injured cells is a fundamental concept to promote regeneration and minimize the extent of injury, but the appropriate cell type for transplantation has not been identified yet for neuromuscular junctions [3]. The discovery of olfactory ecto-mesenchymal stem cells (OE-MSCs) opens a bright horizon to stem cell-based therapies in the future [4]. OE-MSCs are multipotent adult stem cells originated from the neural crest, which could be obtained by simple biopsy of olfactory mucosa resident in the nasal cavity [5,6]. These cells are very interesting in neural tissue engineering, because they (1) have tendency to differentiate into neurons, (2) are free of ethical concerns, and (3) exhibit low immunogenicity, and (4) could be used for autologous transplantation [5,7,8]. However, promoting the differentiation into desirable phenotypes, access to sufficient cell number and survival rate of cells upon transplantation remain the main obstacles in the utilization of stem cell-based therapy [9,10]. To improve the efficiency of transplantation, several recent studies used scaffolds to create a biomimetic microenvironment to enhance the viability of transplanted cells and differentiated them towards specific neural lineages [11,12]. In the past years, various kinds of scaffolds, such as hydrogels, nanofibers and decellularized matrices have been developed for tissue regeneration application [13,14]. Hydrogels provide a suitable porous and interconnected structure for tissue

* Corresponding author at: Applied Biophotonics Research Center, Science and Research Branch, Islamic Azad University, Tehran, Iran.
E-mail address: kamrava.k@iums.ac.ir (S.K. Kamrava).

https://doi.org/10.1016/j.msec.2019.03.068
Received 11 July 2018; Received in revised form 18 March 2019; Accepted 21 March 2019
Available online 25 March 2019
0928-4931/

regeneration, mimicking the hydrated state of extracellular matrix [15,16]. Among possible hydrogels to be developed for tissue regeneration applications, conducting polymers are an efficient tool to control cellular behavior due to their electrical conductivity, which makes them good candidates in neural tissue engineering applications [17–19]. Among conductive polymers, polyaniline (PANI) is very eminent because of its unique and easy doping process, good environmental, thermal, and chemical stability, wide range of conductivity and ease of synthesis [20,21]. However, the hydrophobicity and lack of degradability of PANI restricted its applications in practical biomedical and tissue engineering. These limitations can be overcome by using oligomers of aniline such as aniline pentamer (AP), which have good solubility, biodegradability and electroactivity [22,23]. Moreover, their amine-capped structure makes them suitable to be copolymerized or grafted with other polymers like chitosan and gelatin [24,25]. Pendant amine groups on chitosan repeating unites are attractive domains for grafting of aniline oligomers and improve characteristics such as hydrophilicity, biodegradability, and processability [26]. Additionally, combining AP with gelatin, which is a natural macromolecule with many attractive properties, has already been shown as a promising approach to improve the biological properties of AP [27]. It was reported that the conductive hydrogel based on chitosan-tetraaniline was utilized for muscle and skin regeneration which such hydrogel enhanced the cellular activities and regeneration [28–30]. Electroactive chitosan exhibited the antibacterial properties along with rapid shape memory which can be used as a wound dressing [31,32]. It was reported that the conductivity of the hydrogel has more impact on neural cell activity than hydrogel modulus [33].

In this study, OE-MSCs for the first time were used to investigate their potential ability as an ideal cell source to support motor neuron differentiation on tissue culture polystyrene (TCP), and conductive hydrogel. We hypothesized that the conductivity of AP would increase cell proliferation and differentiation of OE-MSCs into motor neuron-like cells compared to conventional tissue culture plate. These hydrogels could have potential applications in treating neural diseases such as spinal cord injuries.

2. Materials and methods

The materials were purchased from Sigma-Aldrich (USA) unless otherwise noted.

2.1. Synthesis of chitosan-aniline pentamer/gelatin/agarose hydrogel (AP-g-CH/GL/AG)

2.1.1. Synthesis of aniline pentamer (AP)

Aniline pentamer was synthesized according to a method reported in the literature [24]. First, Amino-capped aniline trimer was synthesized by oxidizing aniline and *p*-phenylenediamine by $(NH_4)_2S_2O_8$ in a mixture solution of 1 mol.L^{-1} HCl and acetone. Aniline pentamer was then synthesized by dissolving Amino-capped aniline trimer and *N*, *N*-diphenylamine in a mixture solution of DMF and hydrochloric acid (HCl) with vigorous stirring. To obtain the emeraldine (EM) base form of AP, ammonium persulfate was added to the mixture as an oxidant agent and stirred for 2 h in an ice bath. The EM base form of AP was then reduced with hydrogen at 3 atm platinumoxide for 2 h to produce the fully reduced leucoemeraldine (LM) form of AP. The light gray LM AP was then eluted with distilled water until the filtrate became diaphanous. Finally, it was washed by a Soxhlet extractor with 1,2-dichloroethane and THF to eliminate the excess reducing agent and by-products of the reactions. It was then dried under reduced pressure. In order to obtain carboxyl-capped aniline pentamer, amino groups at the end of EM base form of AP reacted with succinic anhydride and converted to carboxyl groups [34]. The mechanism is schematically showed in Fig. 1.

2.1.2. Synthesis of chitosan-graft-aniline pentamer (AP-g-CH)

0.1 g aniline pentamer, 0.02 g NHS, and 0.03 g EDC were dissolved in 10 ml of DMF and stirred under nitrogen atmosphere for 24 h at room temperature to obtain NHS capped aniline pentamer. The mixture was then added dropwise into the solution of 0.5 g chitosan in 0.1 M HCl and the stirring was brought on for 24 h under the nitrogen atmosphere at 50 °C. After the reaction, the crude product was stored at room temperature for further usages. The AP content in the synthesized AP-g-CH copolymer was 8.9% according to UV–Vis test.

2.1.3. Synthesis of (AP-g-CH/GL/AG)

The solution of 1% wt. of agarose (AG) and gelatin (GL) in distilled water were prepared distinctly. These solutions with the previous AP-g-CH solution were mixed with various volume amount of 0:0:30, 2.5:2.5:25, 5:5:20, 7.5:7.5:15, 10:10:10 where the numbers indicate the volume of AP-g-CH, gelatin, and agarose solutions, respectively (the total volume of each sample was 30 cc). The mixtures were stirred for 20 min and poured into suitable moldes and kept at room temperature overnight. The obtained scaffolds were immersed in ethanol for 48 h under stirring and ethanol was changed every 8 h in order to eliminate unreacted moieties then it was incubated in distilled water for 72 h while the water was replaced every 8 h. Prepared samples are abbreviated as S0, S5, S10, S15, and S20, where the number indicates the summation of the volume of employed AP-g-CH and gelatin (GL) solutions in the AP-g-CH/GL/AG scaffolds. Table 1 also indicates the chemical composition of each sample.

2.2. Characterization of scaffolds

2.2.1. Structural characterization of AP and chitosan-graft-AP

To investigate the successful synthesis of AP and its grafting on the chitosan chains, Fourier-transform infrared (FTIR) spectra of AP and chitosan were recorded in the range of 400–4000 cm^{-1} using a Nicolet 6700 FT-IR spectrometer (Thermo Scientific Instrument).

2.2.2. Swelling and deswelling properties

Swelling kinetic of hydrogels was investigated using a gravimetric method. Specific amounts of dried hydrogels were immersed in distilled water with the pH of 7.2 and their swelling behavior was investigated at various temperatures (30 °C, 40 °C, 50 °C). At pre-determined time intervals, samples were drawn out of the water and weighed after wiping out their superficial water with moistened filter paper until a swelling equilibrium was reached. The swelling ratio was measured according to Eq. (1):

$$SR = \frac{W_s - W_d}{W_d} \times 100\% \quad (1)$$

where W_s, $W_{d,}$ and SR are the weight of the swollen gel at a certain time, the weight of dry gel, and the swelling ratio of hydrogels at a certain time, respectively [35].

The pre-equilibrated samples (in the distilled water with the pH of 7.2 at 30 °C, 40 °C, and 50 °C for 24 h) were weighed in pre-determined time intervals after wiping off the excess surface water. The water retention (WR) of the samples was calculated by Eq. (2):

$$WR = \frac{W_t - W_d}{W_e - W_d} \quad (2)$$

where W_t and W_e are the weight of the hydrogel at a certain time during deswelling and the weight of swollen hydrogel at equlibrium state, respectively [36].

2.2.3. Ionic conductivity

The conductivity of hydrogel samples at their maximum swollen state, which represent the summation of ionic and electronic conductivity, was measured. In order to survey the electronic contribution to the total conductivity, samples were freeze-dried and their electrical

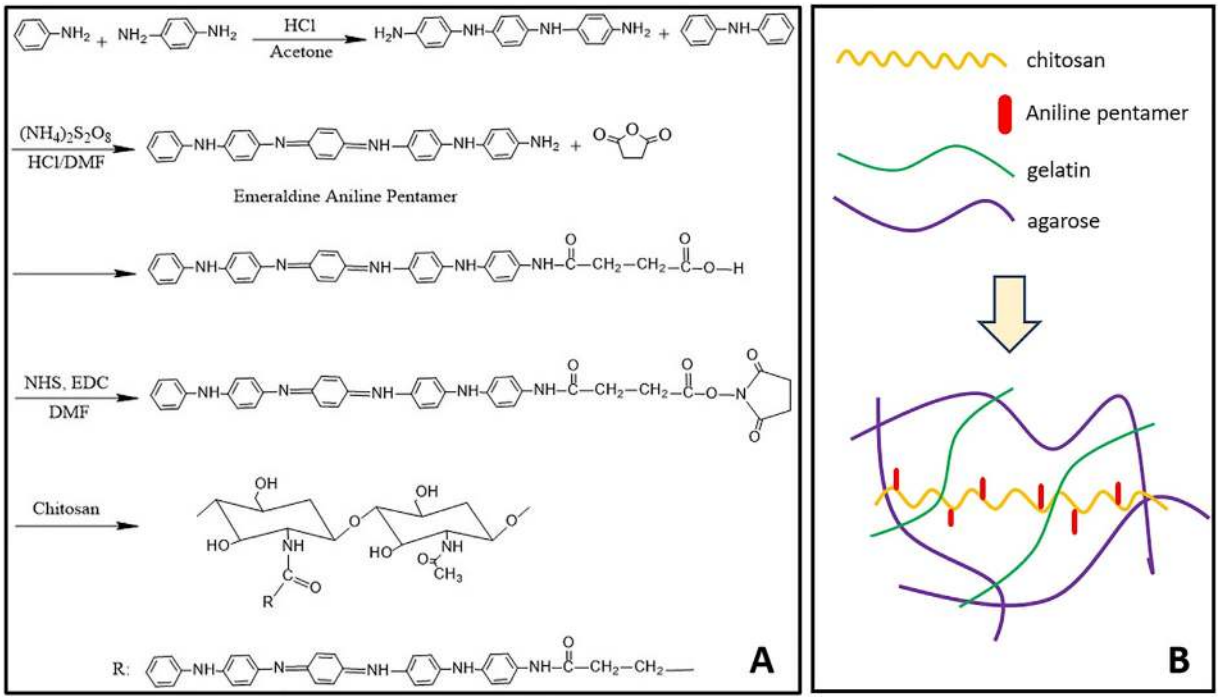

Fig. 1. (A) synthesis of AP-g-CH, (B) schematic mechanism of gel preparation.

Table 1
Chemical composition of synthesized hydrogels. The amount of each solution used for fabricating a hydrogel with total volume of 30 cc is determined.

Sample	Volume of AP-g-CH solution (cc)	Volume of 1% wt GL solution (cc)	Volume of 1% wt AG solution (cc)	Total volume of hydrogel (cc)
S0	0	0	30	30
S5	2.5	2.5	25	30
S10	5	5	20	30
S15	7.5	7.5	15	30
S20	10	10	10	30

conductivity was measured at the dried state (in dried state the ionic conductivity is negligible and the conductivity is equal to electronic conductivity). Ionic conductivity was then calculated by reducing electronic conductivity from total conductivity.

Ionic conductivity of the hydrogels at various temperatures ranging from 30 °C to 80 °C were measured by a two probe techniques. All scaffolds were doped by 1 M HCl before measurements. The specific ionic conductivity (σ) in S.cm^{-1} was measured according to Eq. (3):

$$\sigma = \frac{l}{RA} \tag{3}$$

where *l*, *R* and *A* are specific conductivity, resistance, length and cross sectional area of the composites, respectively.

According to Arrhenius equation, Ln (σT) vs 1000/T was plotted and E_a and A which are the activation energy of conductivity and pre-exponential factor were obtained from the slope and intercept of the diagram. The Arrhenius equation is given by:

$$\sigma = \frac{A}{T}\exp\left(-\frac{E_a}{RT}\right) \tag{4}$$

where σ, T, and R are the ionic conductivity, absolute temperature, the molar gas constant, respectively [37].

2.2.4. Thermal properties

The thermal degradation of the samples was characterized by thermogravimetric analysis (TGA) using a Perkin–Elmer Pyris-1 TGA apparatus. The hydrogels were heated from 50 °C to 700 °C at a heating rate of 10 °C.min^{-1} under a nitrogen atmosphere.

2.2.5. Mechanical assessment

2.2.5.1. Compression stability and elasticity of hydrogel. In order to evaluate mechanical properties of hydrogels, cylindrical shapes with the diameter of 10 mm and thickness of 6 mm were prepared. Uniaxial compression was applied on the hydrogels using Santam-STM200 (Iran) apparatus with a load cell of 10 KN and strain rate of 1 mm. min^{-1} and stress-strain curve was determined.

2.2.5.2. Compression evaluation (shape memory). In order to investigate if the hydrogels have the potential to recover themselves after force loading, shape memory test was implemented. Samples were prepared in cylindrical shape (2 cm height, 10 cm^2 area), and compressed. During compression, hydrogels were deformed, and then they were immersed in water bath to absorb the lost water and recover their initial shape. The compression and recovered deformation were plotted for samples containing various amount of aniline.

2.2.6. Microstructure and morphology evaluation

Morphology of the optimum hydrogel was evaluated using scanning electron microscopy (SEM) in which samples were freeze-dried and coated with gold using a sputter coater. Moreover, porosity of samples was assessed using liquid displacement method. For this aim, freeze-dried hydrogels were immersed in specific volume of hexane (V_1). The total volume of hexane and hydrogel (V_2) was measured. After that, samples were removed and the residual volume of hexane (V_3) was measured and scaffold porosity was measured using Eq. 5.

$$\varepsilon = \frac{V_1 - V_3}{V_2 - V_3} \times 100 \tag{5}$$

2.3. Cell culture

2.3.1. Human olfactory ectomesenchymal stem cell isolation and characterization

Human OE-MSCs were obtained with mechanical method according

to Delorme et al. [4]. Briefly, human nasal mucosa was obtained from 2 males, at Hazrate Rasoul Hospital (Iran University of Medical Sciences); the patient were informed about the experiment and signed consent forms (Tehran, Iran, ethical code: IR.IAU.TMU.REC.1396.177). Briefly, after washing with PBS containing 100 u/ml penicillin and 100 g/ml streptomycin, the biopsies dissected into pieces and placed into a 6-well plate under a sterile glass coverslip and fed with DMEM/F12 medium supplemented with fetal bovine serum (FBS, 10%), penicillin and streptomycin (1%) and the tissues were incubated at 37 °C in 5% CO_2. The culture medium was changed every 2 or 3 days and when the remaining cells reached 80% confluence, the coverslip was removed and the adherent cells were trypsinized and expanded for 3 passages. MSCs derived from nasal mucosa were characterized according to Moayeri et al. using flow cytometry for cell surface markers including CD105, CD90, CD73, CD45, and CD34 and their differentiation capacity towards osteocytes and adipocytes was assessed [38].

2.3.2. Assessment of cell viability on hydrogels

Scaffolds were cut using a biopsy punch, washed three times with PBS and then sterilized with ultraviolet light for 2 h and incubated under standard conditions (a humidified incubator, 37 °C, 5% CO_2) prior to cell seeding. In order to allow the OE-MSCs to attach onto the surface of the porous hydrogel, 10^4 cells/scaffold in 96-well plate were gently laid on top of the scaffold and incubated for 2 h before adding the external culture medium for further incubation. To investigate the viability of cultured cells on the conductive hydrogel and TCP groups, the MTT assay was carried out after 1, 3, and 5 days. Each day, 4 h was taken to incubate the cells in 100 µl solution of MTT dye (0.5 mg/ml stock in solution). After removing MTT, 100 µl DMSO was added to dissolve formazan crystals and shaken for 5 min in dark place. The absorbance of the content of each well was measured at 570 nm using a spectrophotometric plate reader (Expert 96, Asys Hitch, Ec Austria). The experiment was repeated three times and the results were presented as means ± SD.

2.3.3. Directed differentiation of human OE-MSCs into MNs on TCP and scaffolds

We utilized a three phase protocol for MN-like cell differentiation as described previously [39]. OE-MSCs were differentiated by plating 2×10^5 cells onto the scaffolds and TCP and incubated 24 h with pre-induction medium containing DMEM/F12 (1:1), 20% FBS, 2% B27, 10 ng/ml fibroblast growth factor 2 (FGF2), 250 µM isobutylmethylxanthin, and 100 µM 2-metcaptoethanol at 37 °C and 5% CO_2. For inducing motor neuron differentiation, the media was replaced with an induction media supplemented with DMEM/F12 (1:1), 0.2% B27, 100 ng/ml of Shh, and 0.01 ng/ml RA for one week. After 7 days of differentiation, cells were treated with a medium composed of DMEM/F12 (1:1), 0.2% B27 in the presence of neurotrophic factors, including 100 ng/ml glial cell-derived neurotrophic factor (GDNF), and 200 ng/ml brain-derived neurotrophic factor (BDNF) up to 7 days to induce neuronal maturation. A half-volume medium change was performed every 2–3 days.

2.3.4. Quantitative RT-PCR

The Gene expression of neural markers (Nestin, Islet-1, Chat, HB9) and internal control (GAPDH) were performed by quantitative qRT-PCR in treatment groups. Total RNA was extracted from OE-MSCs and differentiated cells using RNeasy Plus Mini Kit (Qiagen, USA) and treated with DNase I (Ambion) to omit other DNAs. Then, the synthesis of complementary DNA (cDNA) from 1 µg of RNA was done based on RevertAid First Strand cDNA Synthesis Kit (Fermentas, USA). Real-time PCR was performed by using 10 µl of SYBR®Green PCR Master Mix (Applied Biosystems, USA), 1 µg of cDNA, 300 nM of forward and reverse primers, and nuclease-free H2O was used to adjust the final volume up to 20 µl. The genes primer sequences used for real-time PCR and annealing temperature are demonstrated in Table 2. All the reactions were done as triplicate. Real-time PCR results were further analyzed using ΔΔCT equation.

Table 2
Primer sequences used in Real time-PCR.

Annealing temp (°C)	Primer sequence(5–3)	Target gene
55	F GCAGGAGAAGACAGCCAACT R AAACCTCAGCTGGTCAT	ChAT
55	F AGCACCAGTTCAAGCTCAACA R ACCAAATCTTCACCTGGGTCTC	Hb-9
56	F ATATCAGGTTGTACGGGTCAAAT R CACGCATCACGAAGTCGTTC	Islet-1
55	F AAAGTTCCAGCTGGCTGTGG R TCCAGCTTGGGGTCCTGAAA	Nestin
55	F TCGCCAGCCGAGCCA R CCTTGACGGTGCCATGGAAT	GAPDH

2.3.5. Immunofluorescent staining

After 15 days induction, to detect the expression of motor neuron-related antigens, the cells were rinsed three times with PBS and fixed in 4% paraformaldehyde during 30 min. After permeabilization with 0.2% Triton X-100 for 30 min, the cells were blocked with 5% bovine serum albumin (BSA) and incubated with primary anti-body against human anti-choline acetyltransferase (Chat; Abcam, 1:200), anti-Islet-1 (Abcam, 1:200), and anti Hb-9 (Santacruz, 1:200), diluted in 5% BSA in PBS overnight. Secondary antibodies included Alexa Fluor 647 donkey anti-goat (1:500) and FITC-donkey anti-rabbit (1:500) and the nuclei were counterstained with DAPI for 3 min at room temperature. The cells were photo-graphed under fluorescent light with a Nikon microscope.

2.3.6. Flow cytometric analysis

In order to quantify protein expression, the expressions of Islet-1, HB9, and Chat proteins at the end of the induction were evaluated by flow cytometry. The treated cells were incubated overnight in the dark at 4 °C with the appropriate primary antibodies followed by 45 min at 37 °C for the secondary antibody. Antibodies used were the same as those for immunofluorescence staining. FACS Calibur flow cytometer (BD BioSciences) was used to detect expressions of these proteins. The results were analyzed using FlowJo software. All flow cytometry samples were performed in triplicate.

2.4. Statistical analysis

The statistical analysis in this study was carried out using Student *t*-test. All assays were performed in triplicate and the data were represented as the mean ± SD. P values < 0.05 were considered as significant.

3. Results and discussion

3.1. Scaffold synthesis and characterization

3.1.1. FT-IR

The FT-IR spectra of AP, CH, and AP-g-CH are represented in Fig. 2. In the IR spectrum of CH, the absorption peaks at 1653 cm^{-1} and 1610 cm^{-1} are corresponded to the C═O stretching of amide groups and N—H bending of amine groups [40]. The IR spectrum of AP exhibits peaks at 3260 cm^{-1} and 3370 cm^{-1} representing the stretching of N—H and OH groups, respectively. The peaks at 1703 cm^{-1} and 1648 cm^{-1} are assigned to the carbonyl groups (–CO–) in –COOH and amide groups (–NHCO–) [40,41]. The 1603 cm^{-1} and 1501 cm^{-1} peaks are attributed to the vibration of benzene ring and quinoid rings, respectively [42]. The absorption peak at 1300 cm^{-1} is ascribed to the C—N stretching in the vicinity of quinoid rings [24,43].

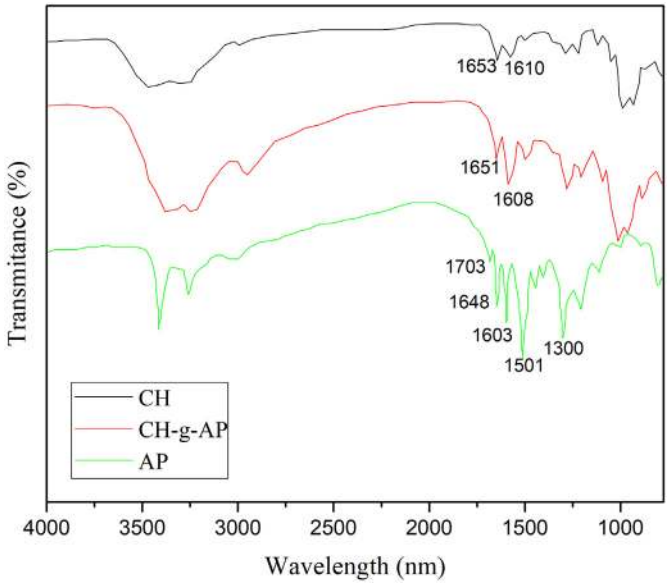

Fig. 2. FTIR spectrum of CH, CH-g-AP, AP.

The FT-IR spectrum of AP-g-CH exhibits all the characteristic peaks of chitosan. Besides, the peak at 1608 cm^{-1} is assigned to the benzene rings of AP. During the coupling of APs on chitosan chains, carboxylic acid groups in Carboxyl-capped Aniline Pentamer react with amine groups of chitosan. Hence, the disappearance of the peak at 1703 which is attributed to the –COOH groups further authenticates the chemical connection of AP to the CH chains.

3.1.2. Swelling/deswelling characterization

Swelling behavior of hydrogels was investigated since the mechanical properties, absorption of physiological fluid, diffusivity of nutrients and drugs in the hydrogel, and the drug release rate is correlated to the swelling capacity of hydrogels [44,45]. Fig. 3a represents the swelling ratio of hydrogels versus time at room temperature revealing that all the hydrogels absorbed water fast at the first minutes of incubation and reached to an equilibrium state thereafter. During the swelling process, water must prevail the osmotic pressure inside the gel in order to permeate in the gel [46]. The osmotic pressure depends on elasticity [36]. Hydrogels have low elasticity in the early phases during swelling. Therefore, the swelling rate is very fast at the beginning. During the swelling process, the amount of absorbed water in the hydrogel increases leading to higher elasticity and thus higher osmotic pressure in the hydrogel. Hence, water needs to overcome higher pressure in order to permeate inside the gel. So, the swelling rate decreases gradually with time. Among hydrogel samples containing AP, S10 and S20 with the swelling ratio of 336.7% ± 13.6 and 215.45% ± 15.5 were the highest and the lowest swelling ratio, respectively. Swelling ratio is proportional to two various parameters: the porosity of hydrogels and the type of polymer. Herein, with increasing AP content, the water absorption is hindered since the amount of free volume between polymer chains reduces and less space is provided for water molecules to be absorbed. In addition to AP content, the amount of each polymer in the hydrogel structure is important since various polymers have different amount of water absorption. For example, gelatin reveals higher water absorption in comparison to agarose and chitosan [47,48]. Consequently, it seems that samples with higher gelatin content show higher water absorption capacity. The summation of these two parameters determines the swelling ratio of the samples. In S10, gelatin content increases the water absorption and the amount of AP was not sufficiently high to restrict the water absorption, thus revealing the highest swelling ratio. On the other hand, in S20 the effect of APs in restricting water absorption was higher than the effect of gelatin in increasing it; so S20 revealed the lowest water absorption.

The deswelling trend of hydrogels is demonstrated in Fig. 3b. The amount of absorbed water by hydrogels decreased fast at the first minutes during deswelling process, and then became slower until reaching the equilibrium state. S10 and S20 represented the highest and the lowest deswelling capacity, respectively.

3.1.3. Conductivity measurements

In order to estimate the conductivity of hydrogels in the body, their conductivity was measured at their maximum swollen state. The conductivity of samples was in the order of 10^{-4} S/cm. This conductivity was attributed to the ionic conductivity, since the electronic conductivity of samples (conductivity at dried state) which was in the range of 1.5×10^{-11} S/cm to 2.91×10^{-11} S/cm, was negligible. This order of ionic conductivity is adequate for conducting micro-currents in the human body to stimulate neural cells proliferation and differentiation [49,50].

Fig. 4a represents the results of conductivity measurements for samples at their maximum swollen state at various temperatures. The conductivity of neat agarose hydrogel at 30 °C increased 20 times by the introduction of AP to its structure (it was 1.41×10^{-5} for neat agarose and 2.86×10^{-4} for S10). The conductivity of neat agarose hydrogel was due to the ionic conductivity of hydroxyl groups on the main chain of agarose. Ionic conductivity increased in the AP-g-CH/GL/AG hydrogels due to the number of ions which were provided for hydrogel by AP. According to literature, the ionic conductivity in the hydrogel samples is a function of two parameters: the number of ions and their

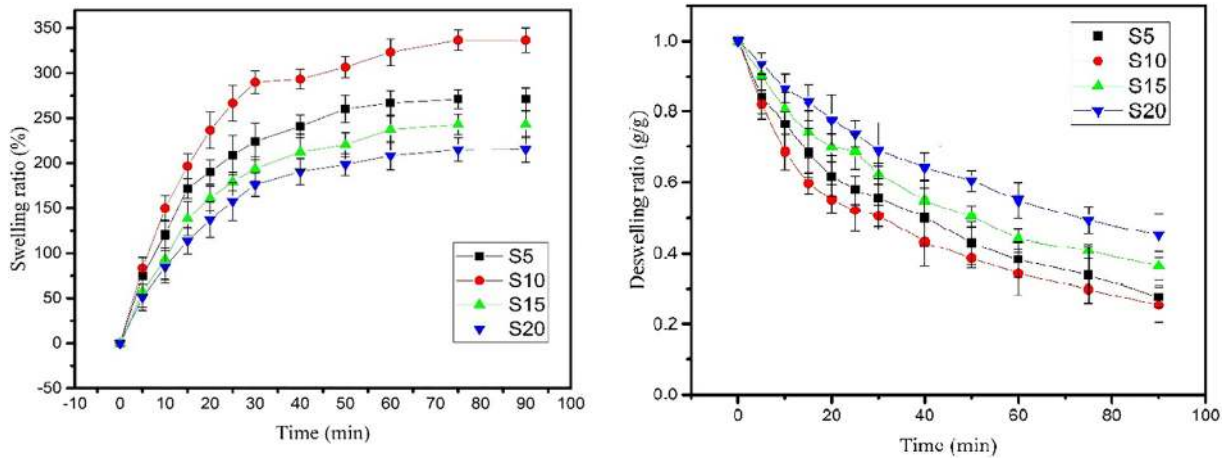

Fig. 3. (a) Swelling and (b) deswelling ratio of AP-g-CH/GL/AG hydrogels with various compositions.

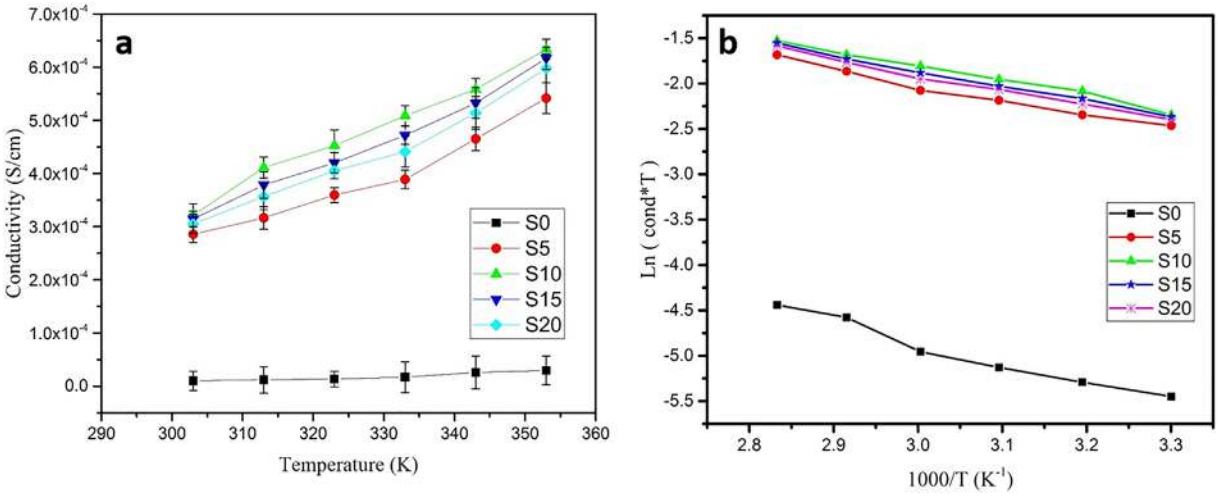

Fig. 4. (a) Ionic conductivity vs temperature (b) Arrhenius plot of AP-g-CH/GL/AG hydrogels with various compositions.

mobility [51,52]. Among samples with AP, S5 had the least ionic conductivity due to its lowest ion content. On the other hand, S10 represented the highest ionic conductivity regarding its highest swelling ratio simplifying ions mobility. Although S15 and S20 had higher ion content, they revealed lower conductivity in comparison to S10 due to their lower swelling capacity suppressing mobility of ions.

Fig. 4b illustrates the Arrhenius plot of Ln (σT) versus 1000/T. This plot showed a linear trend, where the slope of plot multiplied by R represents the activation energy for conductivity and the exponential of the intercept shows the pre-exponential factor. It is implied from the Arrhenius equation that samples with lower activation energy and higher pre-exponential factor have more conductivity. The pre-exponential factor reflects the number of ions in the hydrogel, while activation energy of conductivity reflects the mobility of ions [21]. Herein, according to Table 3, hydrogels with AP content had a higher pre-exponential factor than neat agarose hydrogel because they had higher ion content. Moreover, they had smaller Ea, since less amount of energy was required for ion transfer in them. Among samples with AP content, S10 revealed the smallest activation energy for conductivity. This was justifiable due to its highest swelling capacity leading to easier mobility of ions and S20 revealed the highest Ea due to its lowest swelling ratio and lower ion mobility. The pre-exponential factor was highest for S20 due to the highest number of ions in this hydrogel provided by AP.

3.1.4. Thermal properties characterization

The TGA curves of AP, chitosan, gelatin, agarose, and AP-g-CH/GL/AG hydrogels are shown in Fig. 5. According to TGA curves, the weight loss of hydrogels took place in two stages: a small weight loss in the range of 80 °C to 120 °C, which is due to the evaporation of water and other solvents, and a major weight loss in the range of 300 °C to 350 °C that is ascribed to the degradation of main chains. AP showed higher thermal stability and its major weight loss occurred around 450 °C. Thus, hydrogel samples with higher AP-g-Chi and gelatin content revealed higher thermal stability due to higher thermal stability of AP and gelatin compared with agarose.

Table 3
Data of Arrhenius plot and activation energy of AP-g-CH/GL/AG.

Sample	Slope	Intercept	Activation energy Ea (kJ/mol)	Pre-exponential factor
S0	−2.240	1.873	18.623	6.507791
S5	−1.672	3.0115	13.901	20.31785
S10	−1.656	3.161	13.768	23.59418
S15	−1.689	3.209	14.042	24.75432
S20	−1.724	3.277	14.333	26.49616

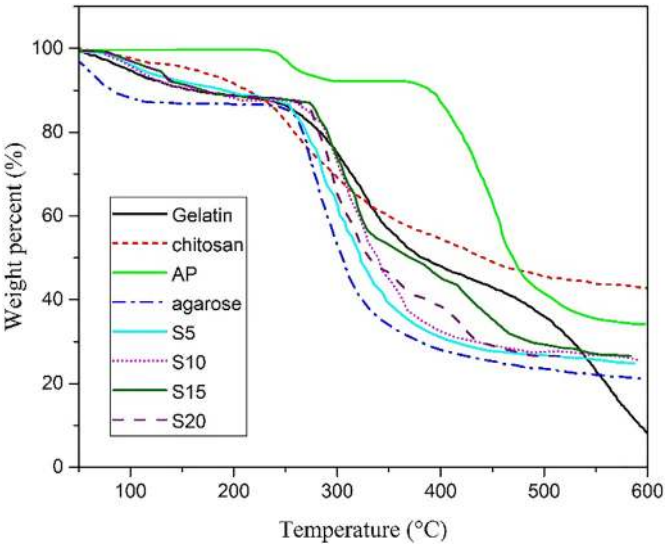

Fig. 5. TGA curves of AP, Chitosan, gelatin, agarose, and AP-g-CH/GL/AG hydrogels.

3.1.5. Mechanical evaluation

Mechanical properties of the scaffold play an important role in tissue regeneration providing integrity to the cells to grow and the ability to withstand the stresses. Fig. 6A reveals the compression strength of the electroactive hydrogel in which aniline pentamer enhanced the hydrogel modulus due to the presence of aromatic ring in the structure and the segmental rigidity. The linear elastic behavior was observed at low and high stress and non-linear elastic behavior was observed at medium stress. The reason for such behavior is that during loading, hydrogel is squeezed and water molecules released out of the gel structure [26]. Hydrogels compression modulus enhanced with aniline pentamer from 32 to 46 KPa; Furthermore, carboxylic groups at the aniline pentamer increased the crosslinking density because of the hydrogen bonding. Shape memory behavior of hydrogels was affected by aniline oligomers content in a way that their compressive strain decreased by aniline content from 31% to 22% (Fig. 6B).

3.1.6. Morphology assessment

Porosity plays an essential role in tissue engineering. High porosity

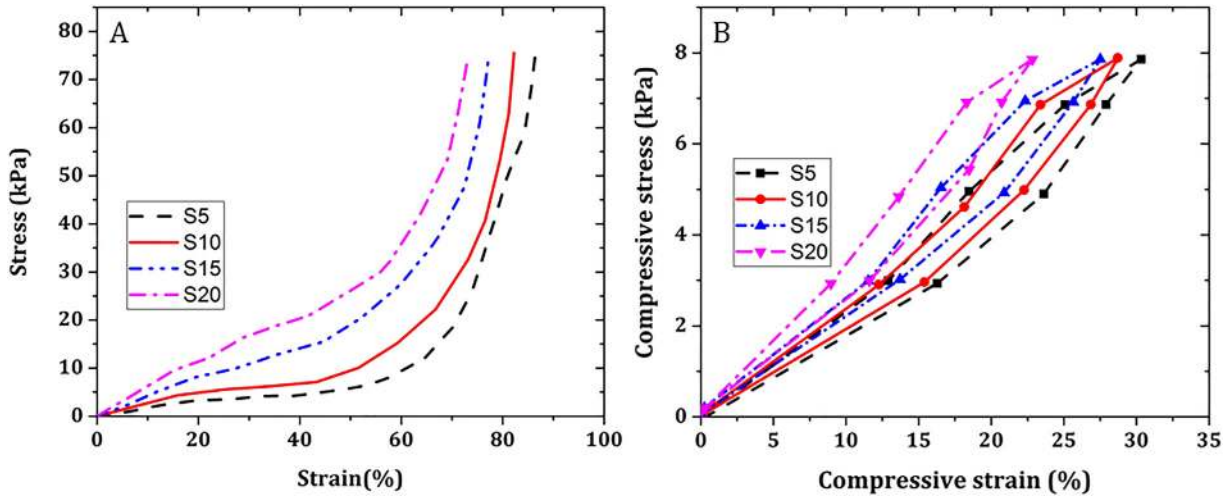

Fig. 6. A) Compression stress of the hydrogels, B) Deformation and recovery of hydrogels.

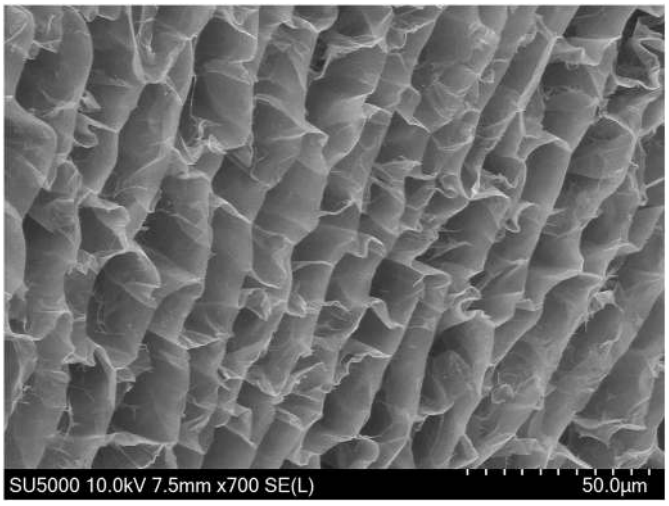

Fig. 7. SEM image of the optimum hydrogel.

of scaffold resulted in higher surface area which helped cells proliferation. Samples´ porosity was about 80% with diameter distribution 35 ± 5 μm which is appropriate for cell growth [53] (Fig. 7).

3.2. Cell isolation and evaluation of cell behavior on scaffolds

3.2.1. Identification of MSCs derived from nasal mocusa

Cell transplantation has been emerged as a promising therapeutic approach to treat a variety of neurological disorders [54]. Among the candidate cells for cell therapy, OE-MSCs are derived easily from olfactory mucosa due to their unique properties such as high proliferation rate and meso-ectodermal origin. These cells have received great attention in neural tissue engineering [4,5,7,55]. In this study, we first showed that OE-MSCs expressed phenotypic markers of mesenchymal stem cell using flow cytometry and then their differentiation capacity towards mesodermal lineage were assessed. The result obtained from flow cytometry analysis demonstrated that the cells were positive for CD90 (98.7), CD105 (97.0), and CD73 (99.2) and negative for CD34 (0.723) and CD45 (0.163) (Fig. 8a). The Fig. 8b shows the spindle shape of the OE-MSCs and their capability to differentiate into adipogenic and osteogenic lineages. Adipogenesis were detected with the visualization of lipid vacuoles stainable with oil red as well as the alizarin red stain, to assessed mineralized calcium. Herein, we used these cells to investigate the effect of conductive hydrogel on their proliferation and differentiation into motor neuron-like cells.

3.2.2. The effect of hydrogels on OE-MSCs proliferation

One of the most important element of the scaffold structure is that it must support cell growth [56]. In this context, in the field of nerve regeneration some attentions have been oriented towards the synthesis of conductive scaffolds, since it was demonstrated that the conductive polymers affect a variety of cell behaviors, such as proliferation and differentiation [57]. Previous works in literature demonstrated the effectiveness of incorporating aniline oligomers as electroactive, biocompatible, and biodegradable moieties in the hydrogel structure [58,59]. However, in this study, apart from using aniline pentamer as conductive moiety, the bioactivity of the scaffold was further improved by using agarose in the hydrogel structure which forms a gel without the need for chemical crosslinkers. Moreover, a combination of chitosan and gelatin as natural polymers enhanced the biocompatibility of this novel hydrogel, Based on the aforementioned results, S10 hydrogel was selected as the optimum hydrogel with the highest ionic conductivity; then, in vitro studies were conducted to judge the proliferation of the cultured OE-MSCs on scaffolds. The results of MTT from day 1 to day 5, as presented in Fig. 9, showed that on the first day of culture cell proliferation on TCP compared to hydrogels was higher but there was no statistically significant difference among them ($P > 0.05$). When incubated for 3 and 5 days, both of the groups proliferated in comparison with day 1, indicating that the hydrogel showed no cytotoxicity effect. After 3 and 5 days of culturing, comparing the cell proliferation showed that cell viability on the hydrogels was significantly higher than TCP ($p < 0.05$ and 0.01), respectively, indicating that the conducting hydrogel facilitated the proliferation of the OE-MSCs during culture period. Since chemical crosslinking agents which are commonly used in the hydrogels, impart some toxicity to the hydrogelin this study, Agarose has been used since it does not need crosslinking agents. It simply forms a gel due to its thermogelling properties [60]. Recent studies have reported the biocompatibility of novel conductive hydrogels based on agarose-aniline pentamer and demonstrated the potential of this scaffolds to stimulate the proliferation of PC12 cells [34]. Hence, it is concluded that employing agarose as a polymer which forms a gel without a crosslinking agent and gelatin as a natural biocompatible polymer in the hydrogel structure made S10 a potentially appealing substrate for proliferation of OE-MSCs.

3.2.3. The analysis of OE-MSCs differentiation into motor neuron like cells on TCP and scaffolds

Degeneration of spinal motor neuron function in a number of devastating neurological disorders results in difficulties in essential

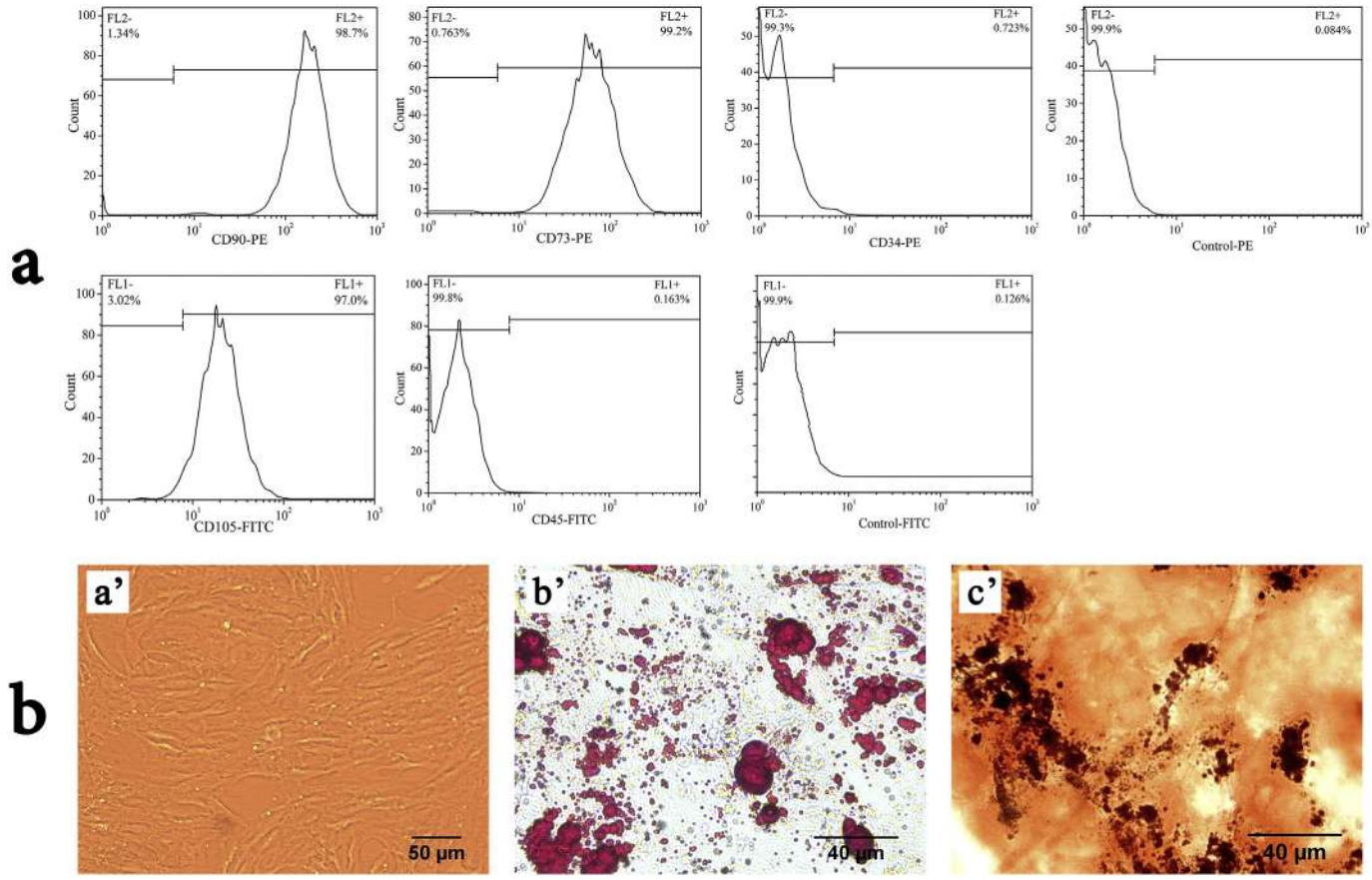

Fig. 8. (a) Flow cytometric analysis of the isolated OE-MSCs at passage 3 revealed that the cells were positive for mesenchymal stem cell markers (CD90, CD73, CD105) and were negative for hematopoietic markers (CD34, CD43). (b) The morphology of the OE-MSCs (a′). OE-MSCs were differentiated into adipocytes (b′) and osteoblasts (c′), and stained with Oil Red O and Alizarin Red, respectively. (For interpretation of the references to colour in this figure legend, the reader is referred to the web version of this article.)

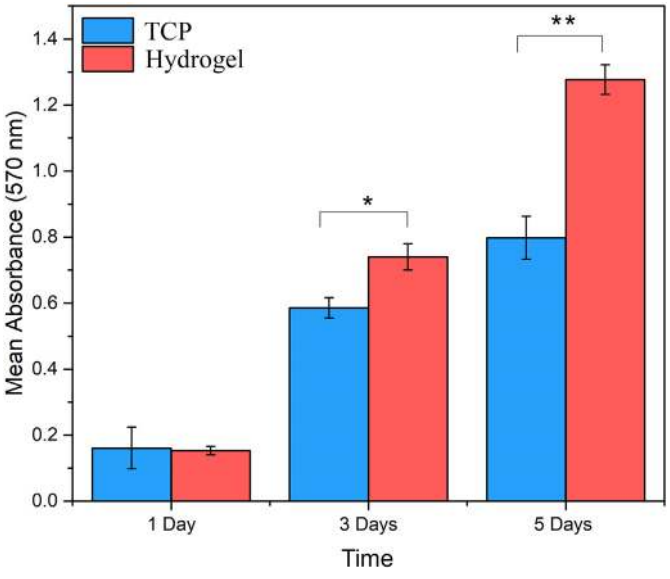

Fig. 9. Determination of viability of the OE-MSCs cultured on hydrogel at three different time points. Formosan absorbance was expressed as a measure of cell viability. The data are expressed as mean ± SD of three independent experiments in duplicate. * $p < 0.05$, ** $p < 0.01$, *** $p < 0.001$.

human behaviors such as muscle movements, including breathing, walking, and swallowing [61]. Exploiting a simple and effective method to produce MNs without any transgenic manipulation in a short time is important for treating motor neuron-related disorders [62]. It was demonstrated that the scaffold conductivity plays an important role for neural tissue engineering and could significantly increase neuronal gene expression without any other external stimuli [33]. In this study, OE-MSCs were used as a new meso-ectodermal cell source for motor neuron-like cell differentiation and we assume that OE-MSCs, which are 100% nestin-positive [63,64], have better tendency to differentiate into neuron cells compared to MSCs. OE-MSCs were seeded in the presence of neural inductive molecules on scaffolds and TCP plates for 2 weeks and the characterization of differentiated cells performed via Real-time PCR, immunostaining, and flow cytometry. We hypothesized that AP-g-CH/GL/AG hydrogels due to their high water content, thermal stability, biocompatiblity, and conductivity of about 10^{-4} S/cm provide an optimal microenvironment for cell proliferation and neural differentiation.

As shown in Fig. 10, quantitative RT-PCR analysis revealed that cells not only expressed neural progenitors such as nestin, but also expressed transcription factors including ISL1, HB9, and Chat which are MN markers [65]. Previous studies have shown the potential of MSCs from various sources to differentiate into MN-like cells under certain media conditions [2,39,66]. Gene expression at day 15 showed that the expression of nestin, a marker of neural progenitor cells, decreased compared to TCP group at the end of the induction, while the expression of MN marker increased. The expression of motor neuron markers such as ISL1, HB9, and Chat were 12.52 ± 0.42, 20.45 ± 1.90, and 15.26 ± 3.03 times, respectively, which were statically significant compared to differentiated cells on TCP groups (*$p < 0.05$).

It should be noted that although OE-MSCs could differentiate into MN-like cells in the present of induction media in TCP groups,

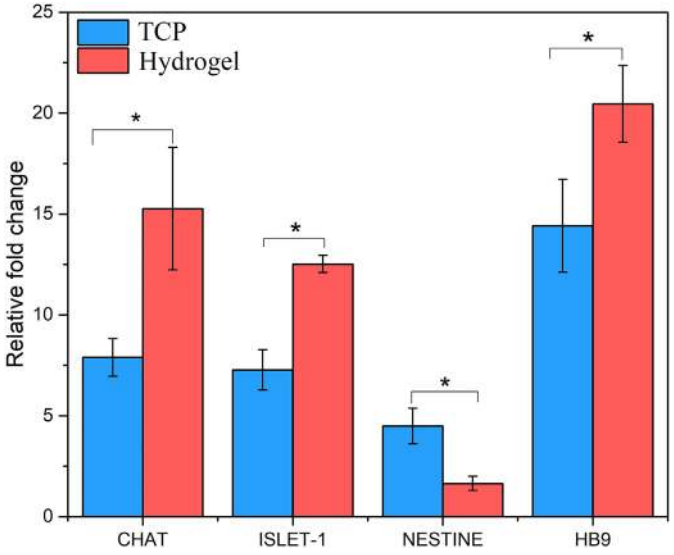

Fig. 10. Relative mRNA expression using real-time PCR for the detection of motor neuron-like cells markers on conductive hydrogel versus TCP samples. GAPDH is used as a housekeeping gene control. ($n = 3$ biological samples, mean ± SD).

conductive hydrogels provided further than only a passive supporting structure for the cells and could influence stem cells fate by inducing their differentiation. Increasing evidence has recently highlighted that the structural properties of scaffolds affect cell behavior [67,68] and conductive hydrogels in this study, as an artificial substrate, are able to promote cell proliferation and neural differentiation. In this study, we used a combination of RA, Shh, BDNF, and GDNF for the induction of MNs from human OE-MSCs on TCP and conductive hydrogels for 2 weeks. RA and Shh which induce acquisition of caudal and ventralization identity, respectively, are the most important signals specifying the ventral spinal fate [69]. We have previously reported in vitro differentiation of Wharton's jelly-derived mesenchymal stem cells towards MN-like cells on TCP and nanofibers scaffolds resulting in a positive effect of the nanofibrous scaffold on MN-like cells [56]. In another study, Ebrahimi-Barough et al. suggested PLGA nanofiber scaffolds as a suitable substrate to induce the human endometrial stem cells into MN-like cells [70]. Although other researchers have also been differentiated stem cells into motor neurons on different scaffolds in several previous studies [71,72], there is no report investigating the effect of conductive hydrogels on MN differentiation. Here, to confirm the real-time PCR results immunofluorescent staining and flow cytometry analysis were used to examine the expression of MN specific markers at protein levels. Immunocytochemistry confirmed that the cells were positive for both ISL1 and HB9 proteins, which seems to indicate that the expression is enhanced in hydrogels than on TCP (Fig. 11).

Evaluating the percentage of MN markers (Islet-1, Chat and HB9) by flow cytometer revealed a remarkable increase in the number of positive cells on conductive hydrogels versus TCP groups (Fig. 12). The expression of Islet-1 (36.33% ± 2.61), Chat (34.46% ± 1.55) and HB9 (54.43% ± 1.55) in conductive hydrogels was higher than the expression of Islet-1 (22.8% ± 2.98), Chat (21.5% ± 0.85) and HB9 (30.73% ± 1.097) on TCP groups ($P < 0.05$, 0.01 and 0.001), respectively.

HB9 as a homeobox gene expressed selectively by MNs at the late phases of the motor neuron differentiation [73]. Reinhardt et al. have used small molecules of human neural progenitor and enabled to improve the efficiency of pure HB9 motor neurons to 50% within 30 days [74]. Interestingly, the result of the flow cytometry in this study showed that OE-MSCs could generate similar percentage of HB9 in only 2 weeks on scaffolds. In other studies, MNs were induced from human pluripotent stem cells with adenoviral gene delivery. This approach could produce mature MNs in a short time and with high efficacy, it needs genetic manipulations which are difficult to control in a precise manner and is also a time-consuming process [75]. In this study, tissue engineering strategies succeeded to induce the transition of progenitor cells into motor neuron-like cells in a short time by providing a biomimetic environment enhancing the efficiency of cell differentiation. We hypothesized that our success to achieve derivation of MNs specific markers within a short culture period can be attributed to the following reasons: 1) the neural crest origin of OE-MSCs which indicates the tendency of these cells to differentiate into the neural lineage [5,7] 2) incorporation of AP in the hydrogel structure provides sufficient conductivity which induces neural differentiation [34]. It should be emphasized that although the conductive hydrogels used in this study are potential scaffolds to induce OE-MSCs differentiation into MN-like cells, further studies are needed to evaluate the complete maturation of cell differentiation. Given the ability of conductive hydrogel used in this study to support OE-MSCs proliferation and differentiation into MN cells, we next wished to examine the potential of this construct in an animal model of spinal cord injury (SCI) and we hope to develop effective treatments for MN-related disorders.

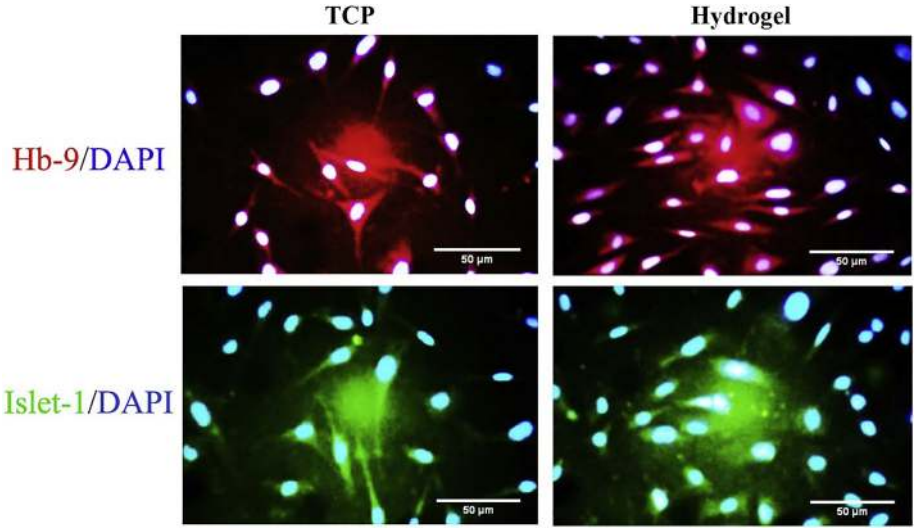

Fig. 11. Immunocytochemical analysis for expression of HB9 and Islet-1 as markers of mature and progenitor motor neurons, respectively.

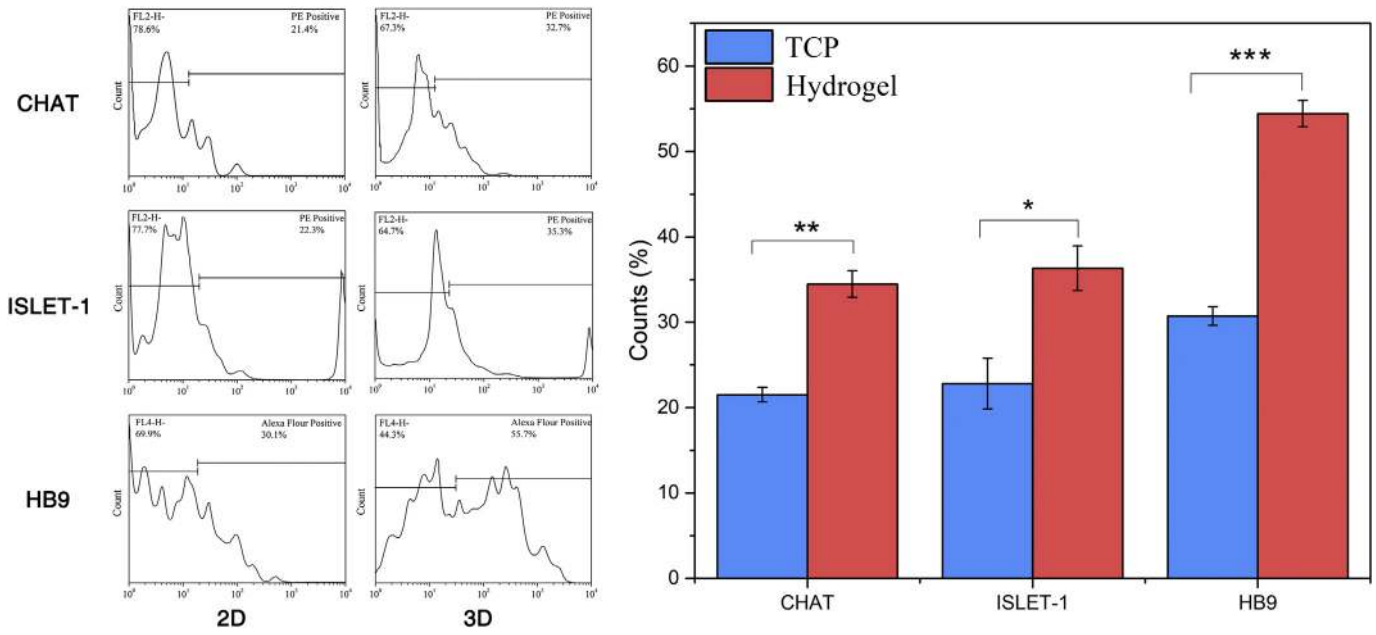

Fig. 12. Cytofluorimetric analysis revealed that after induction, the level of the motor neuron-specific-protein including Islet-1, Chat, and HB9 on conductive hydrogel scaffolds increase in comparison to TCP group.

4. Conclusion

In this study, chitosan-aniline pentamer/gelatin/agarose hydrogels with different concentrations were synthesized and characterized successfully. All samples showed appropriate swelling ratio and electrical conductivity highlighting the fact that AP is a potential conductive moiety to be used in hydrogels for tissue engineering applications. Among all samples, the one with 10% AP-g-CH/GL revealed the highest conductivity. This highest conductivity was attributed to the highest swelling ratio, which provides more free space for ions to move faster. This hydrogel exhibited a ionic conductivity in the order of 10^{-4} S/m, which is adequate for conducting micro-currents in the human body and stimulating neural cells proliferation and differentiation. Thermal property measurements revealed that thermal stability of hydrogels improve with AP content due to the higher thermal stability of AP. S10 as the sample with best swelling and ionic conductivity was chosen for further investigation tests. Quantitative real-time PCR, immunocytochemistry staining, and flow cytometry analysis was utilized to evaluate the efficacy of the hydrogel to induce OE-MSCs to motor neuron-like cells. Islet-1, HB-9, and Chat which are known as MN markers according to literature, revealed significant increase in RNA and protein level in comparison to TCP. All these results suggest that the developed conductive hydrogels provide a desirable microenvironment for proliferation and MN-like cells differentiation of OE-MSCs, demonstrating their great potential to treat MN-related diseases.

Acknowledgments

The financial support of the Research and Technology Council of the Science and Research Branch of Islamic Azad University is gratefully acknowledged. Authors are also grateful for the close cooperation of the Iranian Research Assist Company in improving the following research's results.

References

[1] F. Faghihi, et al., Differentiation potential of human bone marrow mesenchymal stem cells into motorneuron-like cells on electrospun gelatin membrane, J. Mol. Neurosci. 55 (4) (2015) 845–853.
[2] F. Faghihi, et al., Differentiation potential of human chorion-derived mesenchymal stem cells into motor neuron-like cells in two-and three-dimensional culture systems, Mol. Neurobiol. 53 (3) (2016) 1862–1872.
[3] R. Alizadeh, S. Mehrabi, M. Hadjighassem, Cell therapy in Parkinson's disease, Arch. Neurosci. 1 (2) (2013) 43–50.
[4] B. Delorme, et al., The human nose harbors a niche of olfactory ectomesenchymal stem cells displaying neurogenic and osteogenic properties, Stem Cells Dev. 19 (6) (2009) 853–866.
[5] A. Wetzig, A. Mackay-Sim, W. Murrell, Characterization of olfactory stem cells, Cell Transplant. 20 (11 − 12) (2011) 1673–1691.
[6] R. Alizadeh, et al., Human olfactory stem cells: as a promising source of dopaminergic neuron-like cells for treatment of Parkinson's disease, Neurosci. Lett. 696 (2019) 52–59.
[7] Z. Zhang, et al., Nasal ectomesenchymal stem cells: multi-lineage differentiation and transformation effects on fibrin gels, Biomaterials 49 (2015) 57–67.
[8] Z. Bagher, et al., Differentiation of neural crest stem cells from nasal mucosa into motor neuron-like cells, J. Chem. Neuroanat. 92 (2018) 35–40.
[9] S. Karimi-Abdolrezaee, et al., Delayed transplantation of adult neural precursor cells promotes remyelination and functional neurological recovery after spinal cord injury, J. Neurosci. 26 (13) (2006) 3377–3389.
[10] A.M. Parr, I. Kulbatski, C.H. Tator, Transplantation of adult rat spinal cord stem/progenitor cells for spinal cord injury, J. Neurotrauma 24 (5) (2007) 835–845.
[11] Z. Bagher, et al., Differentiation of Wharton's jelly-derived mesenchymal stem cells into motor neuron-like cells on three-dimensional collagen-grafted nanofibers, Mol. Neurobiol. 53 (4) (2016) 2397–2408.
[12] B. Bakhshandeh, et al., Tissue engineering; strategies, tissues, and biomaterials, Biotechnol. Genet. Eng. Rev. 33 (2) (2017) 144–172.
[13] A. Subramanian, U.M. Krishnan, S. Sethuraman, Development of biomaterial scaffold for nerve tissue engineering: biomaterial mediated neural regeneration, J. Biomed. Sci. 16 (1) (2009) 108.
[14] P. Zarrintaj, et al., Poloxamer-based stimuli-responsive biomaterials, Materials Today: Proceedings 5 (7) (2018) 15516–15523.
[15] U.P. Shinde, B. Yeon, B. Jeong, Recent progress of in situ formed gels for biomedical applications, Prog. Polym. Sci. 38 (3–4) (2013) 672–701.
[16] M. Salehi, et al., Alginate/chitosan hydrogel containing olfactory ectomesenchymal stem cells for sciatic nerve tissue engineering, J. Cell. Physiol. (2019), https://doi.org/10.1002/jcp.28183 (Epub ahead of print).
[17] Y. Wu, et al., Interwoven aligned conductive nanofiber yarn/hydrogel composite scaffolds for engineered 3D cardiac anisotropy, ACS Nano 11 (6) (2017) 5646–5659.
[18] B. Guo, P.X. Ma, Conducting polymers for tissue engineering, Biomacromolecules 19 (6) (2018) 1764–1782.
[19] P. Zarrintaj, et al., Polyaniline in retrospect and prospect, Materials Today: Proceedings 5 (7) (2018) 15852–15860.
[20] Y.A. Ismail, et al., Electrochemical actuation in chitosan/polyaniline microfibers for artificial muscles fabricated using an in situ polymerization, Sensors Actuators B Chem. 129 (2) (2008) 834–840.
[21] V. Ivanov, et al., Template synthesis of polyaniline in the presence of poly-(2-acrylamido-2-methyl-1-propanesulfonic acid), Russ. J. Electrochem. 40 (3) (2004) 299–304.
[22] P. Zarrintaj, et al., Oligoaniline-based conductive biomaterials for tissue engineering, Acta Biomater. 72 (2018) 16–34.
[23] P. Zarrintaj, et al., A facile route to the synthesis of anilinic electroactive colloidal

hydrogels for neural tissue engineering applications, J. Colloid Interface Sci. 516 (2018) 57–66.
[24] L. Zhang, et al., Non-cytotoxic conductive carboxymethyl-chitosan/aniline pentamer hydrogels, React. Funct. Polym. 82 (2014) 81–88.
[25] L. Li, et al., In situ forming biodegradable electroactive hydrogels, Polym. Chem. 5 (8) (2014) 2880–2890.
[26] Z. Atoufi, et al., A novel bio electro active alginate-aniline tetramer/agarose scaffold for tissue engineering: synthesis, characterization, drug release and cell culture study, J. Biomater. Sci. Polym. Ed. 28 (15) (2017) 1617–1638.
[27] M. Li, et al., Electrospinning polyaniline-contained gelatin nanofibers for tissue engineering applications, Biomaterials 27 (13) (2006) 2705–2715.
[28] B. Guo, et al., Degradable conductive self-healing hydrogels based on dextran-graft-tetraaniline and N-carboxyethyl chitosan as injectable carriers for myoblast cell therapy and muscle regeneration, Acta Biomater. 84 (2019) 180–193.
[29] J. Qu, et al., Degradable conductive injectable hydrogels as novel antibacterial, anti-oxidant wound dressings for wound healing, Chem. Eng. J. 362 (2019) 548–560.
[30] S. Mohebbi, et al., Chitosan in biomedical engineering: a critical review, Curr. Stem Cell Res. Ther. (2018), https://doi.org/10.2174/1574888X13666180912142028 (Epub ahead of print).
[31] X. Zhao, et al., Injectable antibacterial conductive nanocomposite cryogels with rapid shape recovery for noncompressible hemorrhage and wound healing, Nat. Commun. 9 (1) (2018) 2784.
[32] J. Qu, et al., Antibacterial adhesive injectable hydrogels with rapid self-healing, extensibility and compressibility as wound dressing for joints skin wound healing, Biomaterials 183 (2018) 185–199.
[33] Y. Wu, et al., Electroactive biodegradable polyurethane significantly enhanced Schwann cells myelin gene expression and neurotrophin secretion for peripheral nerve tissue engineering, Biomaterials 87 (2016) 18–31.
[34] P. Zarrintaj, et al., A novel electroactive agarose-aniline pentamer platform as a potential candidate for neural tissue engineering, Sci. Rep. 7 (1) (2017) 17187.
[35] M. Sadeghi, H. Hosseinzadeh, Synthesis and properties of collagen-g-poly (sodium acrylate-co-2-hydroxyethylacrylate) superabsorbent hydrogels, Braz. J. Chem. Eng. 30 (2) (2013) 379–389.
[36] Z. Zhao, et al., Swelling/deswelling kinetics of PNIPAAm hydrogels synthesized by microwave irradiation, Chem. Eng. J. 142 (3) (2008) 263–270.
[37] A.N. Cormack, Mass transport in anion deficient fluorite oxides, Materials Science Forum, Trans Tech Publ, 1986.
[38] A. Moayeri, et al., Transdifferentiation of human dental pulp stem cells into oligoprogenitor cells, Basic Clin. Neurosci. 8 (5) (2017) 387.
[39] Z. Bagher, et al., Induction of human umbilical Wharton's jelly-derived mesenchymal stem cells toward motor neuron-like cells, In Vitro Cell. Dev. Biol. Anim. 51 (9) (2015) 987–994.
[40] X. Ma, et al., Nanofibrous electroactive scaffolds from a chitosan-grafted-aniline tetramer by electrospinning for tissue engineering, RSC Adv. 4 (26) (2014) 13652–13661.
[41] B. Guo, A. Finne-Wistrand, A.-C. Albertsson, Enhanced electrical conductivity by macromolecular architecture: hyperbranched electroactive and degradable block copolymers based on poly (ε-caprolactone) and aniline pentamer, Macromolecules 43 (10) (2010) 4472–4480.
[42] L. Huang, et al., Synthesis and characterization of electroactive and biodegradable ABA block copolymer of polylactide and aniline pentamer, Biomaterials 28 (10) (2007) 1741–1751.
[43] T.-C. Huang, et al., Aniline pentamer-based electroactive polyimide prepared from oxidation coupling polymerization for electrochemical sensing application, Polymer 53 (20) (2012) 4373–4379.
[44] H. Hezaveh, et al., Swelling behaviour and controlled drug release from cross-linked κ-carrageenan/NaCMC hydrogel by diffusion mechanism, J. Microencapsul. 29 (4) (2012) 368–379.
[45] H. Gasmi, et al., Does PLGA microparticle swelling control drug release? New insight based on single particle swelling studies, J. Control. Release 213 (2015) 120–127.
[46] J. Sun, et al., Synthesis and characterization of a pH-sensitive hydrogel made of pyruvic-acid-modified chitosan, J. Biomater. Sci. Polym. Ed. 18 (1) (2007) 35–44.
[47] P. Zarrintaj, et al., Agarose-based biomaterials for tissue engineering, Carbohydr. Polym. 187 (2018) 66–84.
[48] S.P. Miguel, et al., Thermoresponsive chitosan–agarose hydrogel for skin regeneration, Carbohydr. Polym. 111 (2014) 366–373.
[49] V. Guarino, et al., Conductive PANi/PEGDA macroporous hydrogels for nerve regeneration, Adv. Healthc. Mater. 2 (1) (2013) 218–227.
[50] J. Niple, et al., A portable meter for measuring low frequency currents in the human body, Bioelectromagnetics 25 (5) (2004) 369–373.
[51] W. Zhao, et al., Facile and green approach towards electrically conductive hemicellulose hydrogels with tunable conductivity and swelling behavior, Chem. Mater. 26 (14) (2014) 4265–4273.
[52] M. Petrowsky, R. Frech, Salt concentration dependence of the compensated Arrhenius equation for alcohol-based electrolytes, Electrochim. Acta 55 (4) (2010) 1285–1288.
[53] I. Bružauskaitė, et al., Scaffolds and cells for tissue regeneration: different scaffold pore sizes—different cell effects, Cytotechnology 68 (3) (2016) 355–369.
[54] R. Alizadeh, et al., In vitro differentiation of neural stem cells derived from human olfactory bulb into dopaminergic-like neurons, Eur. J. Neurosci. 45 (6) (2017) 773–784.
[55] A.D. Veron, et al., Isolation and characterization of olfactory ecto-mesenchymal stem cells from eightmammalian genera, BMC Vet. Res. 14 (1) (2018) 17, https://doi.org/10.1186/s12917-018-1342-2.
[56] Z. Bagher, et al., Cellular activity of Wharton's Jelly-derived mesenchymal stem cells on electrospun fibrous and solvent-cast film scaffolds, J. Biomed. Mater. Res. A 104 (1) (2016) 218–226.
[57] H. Park, et al., Effects of electrical stimulation in C2C12 muscle constructs, J. Tissue Eng. Regen. Med. 2 (5) (2008) 279–287.
[58] H. Cui, et al., Synthesis of biodegradable and electroactive tetraaniline grafted poly (ester amide) copolymers for bone tissue engineering, Biomacromolecules 13 (9) (2012) 2881–2889.
[59] Y. Liu, et al., Synthesis and characterization of novel biodegradable and electroactive hydrogel based on aniline oligomer and gelatin, Macromol. Biosci. 12 (2) (2012) 241–250.
[60] J.-Y. Xiong, et al., Topology evolution and gelation mechanism of agarose gel, J. Phys. Chem. B 109 (12) (2005) 5638–5643.
[61] R. López-González, I. Velasco, Therapeutic potential of motor neurons differentiated from embryonic stem cells and induced pluripotent stem cells, Arch. Med. Res. 43 (1) (2012) 1–10.
[62] Q. Qu, et al., High-efficiency motor neuron differentiation from human pluripotent stem cells and the function of Islet-1, Nat. Commun. 5 (2014) 3449.
[63] R. Alizadeh, et al., Differentiation of human mesenchymal stem cells (MSC) to dopaminergic neurons: a comparison between Wharton's Jelly and olfactory mucosa as sources of MSCs, J. Chem. Neuroanat. 96 (2019) 126–133.
[64] S.L. Lindsay, S.C. Barnett, Are nestin-positive mesenchymal stromal cells a better source of cells for CNS repair? Neurochem. Int. 106 (2017) 101–107.
[65] H.J. Lee, et al., Human motor neurons generated from neural stem cells delay clinical onset and prolong life in ALS mouse model, PLoS One 9 (5) (2014) e97518.
[66] S. Shirian, et al., Comparison of capability of human bone marrow mesenchymal stem cells and endometrial stem cells to differentiate into motor neurons on electrospun poly (ε-caprolactone) scaffold, Mol. Neurobiol. 53 (8) (2016) 5278–5287.
[67] N.D. Leipzig, M.S. Shoichet, The effect of substrate stiffness on adult neural stem cell behavior, Biomaterials 30 (36) (2009) 6867–6878.
[68] A. Banerjee, et al., The influence of hydrogel modulus on the proliferation and differentiation of encapsulated neural stem cells, Biomaterials 30 (27) (2009) 4695–4699.
[69] T.M. Jessell, Neuronal specification in the spinal cord: inductive signals and transcriptional codes, Nat. Rev. Genet. 1 (1) (2000) 20.
[70] S. Ebrahimi-Barough, et al., Evaluation of motor neuron-like cell differentiation of hEnSCs on biodegradable PLGA nanofiber scaffolds, Mol. Neurobiol. 52 (3) (2015) 1704–1713.
[71] L. Binan, et al., Differentiation of neuronal stem cells into motor neurons using electrospun poly-L-lactic acid/gelatin scaffold, Biomaterials 35 (2) (2014) 664–674.
[72] N. Bahrami, et al., Purmorphamine as a Shh signaling activator small molecule promotes motor neuron differentiation of mesenchymal stem cells cultured on nanofibrous PCL scaffold, Mol. Neurobiol. 54 (7) (2017) 5668–5675.
[73] S. Arber, et al., Requirement for the homeobox gene Hb9 in the consolidation of motor neuron identity, Neuron 23 (4) (1999) 659–674.
[74] P. Reinhardt, et al., Derivation and expansion using only small molecules of human neural progenitors for neurodegenerative disease modeling, PLoS One 8 (3) (2013) e59252.
[75] M.E. Hester, et al., Rapid and efficient generation of functional motor neurons from human pluripotent stem cells using gene delivered transcription factor codes, Mol. Ther. 19 (10) (2011) 1905–1912.